American Journal of Botany 91(3): 386–400. 2004.

ANALYSIS OF CIRCULAR BORDERED PIT FUNCTION II. GYMNOSPERM TRACHEIDS WITH TORUS-MARGO PIT MEMBRANES[1]

UWE G. HACKE,[2] JOHN S. SPERRY, AND JARMILA PITTERMANN

Biology Department, University of Utah, 257 South 1400 East, Salt Lake City, Utah 84112 USA

A model of xylem conduit function was applied to gymnosperm tracheids with torus-margo pit membranes for comparison with angiosperm vessels. Tracheids from 17 gymnosperm tree species with circular bordered pits and air-seed pressures from 0.8 to 11.8 MPa were analyzed. Tracheids were more reinforced against implosion than vessels, consistent with their double function in transport and support. Tracheid pits were 3.3 to 44 times higher in hydraulic conductivity than vessel pits because of greater membrane conductivity of the torus-margo configuration. Tight scaling between torus and pit size maximized pit conductivity. Higher pit conductivity allowed tracheids to be 1.7–3.4 times shorter than vessels and still achieve 95% of their lumen-limited maximum conductivity. Predicted tracheid lengths were consistent with measured lengths. The torus-margo structure is important for maximizing the conductivity of the inherently length-limited tracheid: replacing the torus-margo membrane with a vessel membrane caused stem tracheid conductivity to drop by 41%. Tracheids were no less hydraulically efficient than vessels if they were long enough to reach their lumen-limiting conductivity. However, this may only be possible for lumen diameters below approximately 60–70 μm.

Key words: functional wood anatomy; hydraulic architecture; plant biomechanics; plant water transport; tracheids; xylem cavitation; xylem hydraulic conductivity.

The secondary xylem of gymnosperms and angiosperms accomplishes the same functions of water transport and mechanical support, but with very different wood structure. This second of two papers completes a comparative analysis of water transport in these contrasting wood types.

Gymnosperm wood is superficially simple, composed mostly of the single-celled tracheid that functions both as a conduit for water flow and for providing mechanical strength to the axis. The intertracheid pits, however, are quite specialized. These are usually circular bordered pits with a torus-margo pit membrane (Bauch et al., 1972). The torus-margo differentiation is a unique compromise to the conflict between allowing water flow between functional tracheids while preventing air flow from an embolized tracheid. The thin and porous margo provides passage for water (Fig. 1A), yet traps an air-water meniscus by capillary action. The capillary suction aspirates the membrane, and the thickened torus seals off the aperture to provide the final barrier to air movement (Fig. 1B). This valve is good up to a certain pressure difference, the ''air-seed pressure,'' at which air leaks past and nucleates cavitation in the adjacent tracheid. The available evidence suggest that the torus is pulled through the aperture, exposing the margo (Sperry and Tyree, 1990). Whether this happens by elastic stretching of the margo (''stretch-seeding'') or by actual rupture of the margo (''rupture-seeding'') is unknown (Fig. 1C). In latewood tracheids, in which the torus and margo can be less well differentiated, air seeding may occur through margo pores without membrane aspiration (Domec and Gartner, 2002).

Angiosperm wood, with its multicellular vessels for transport and fibers for mechanical strength, has more cell types than gymnosperm wood. However, its intervessel pitting is less specialized. The pit membrane is generally homogenous in thickness and porosity, and it is a much simpler valve. Water flows through the evenly distributed fine pores of the membrane (Fig. 1A), and these fine pores also trap an air–water interface. There is no torus, and the sealing of the pit depends entirely on the capillary forces generated at the same pores through which the water flows (Fig. 1B). Consequently, these pores must be much smaller than the pores of the gymnosperm margo. Air-seeding can occur either by the failure of the capillary forces in the preexisting membrane pores (capillary-seeding) or through pores created by structural failure of the membrane (rupture-seeding, Fig. 1C).

In the first paper of this series (Sperry and Hacke, 2004), we showed that angiosperm pitting had relatively low hydraulic conductivity. However, this low conductivity could be overcome if vessels achieved a certain ''saturating length.'' At this length, the vessel conductivity per unit length and per wall area is determined only by the lumen size and wall thickness, canceling out any direct effect of pit conductivity. Achieving the saturating conduit length may be no problem for the multicellular vessel. The optimal vessel length should be the saturating length because at this point conductivity has been maximized, and the disadvantages of excessive length (loss of conductivity by cavitation, damage, and vascular disease) is minimized (Comstock and Sperry, 2000). In support of this hypothesis, predicted saturating lengths were consistent with observed lengths. Pit structure also came closest to achieving the maximum possible vessel conductivity for vessels at their saturating length.

We also showed that vessels maintained a fairly modest safety factor against wall collapse by negative pressure. Predicted implosion pressures were only about twice the air-seed pressure. The advantage of such modest safety factors may be in minimizing the wall thickness for a given cavitation pressure. Thin walls are more economical and achieve a greater vessel conductivity per unit wall area invested in transport.

In this second paper, we subject the gymnosperm tracheid

[1] Manuscript received 1 July 2003; revision accepted 21 October 2003.

The authors wish to thank Professor Larry DeVries of the University of Utah Mechanical Engineering Department and Fred Adler of the University of Utah Biology Department for numerous discussions concerning the modeling of stresses and strains in the xylem. This research was supported by NSF grant IBN-0112213.

[2] E-mail: hacke@biology.utah.edu.

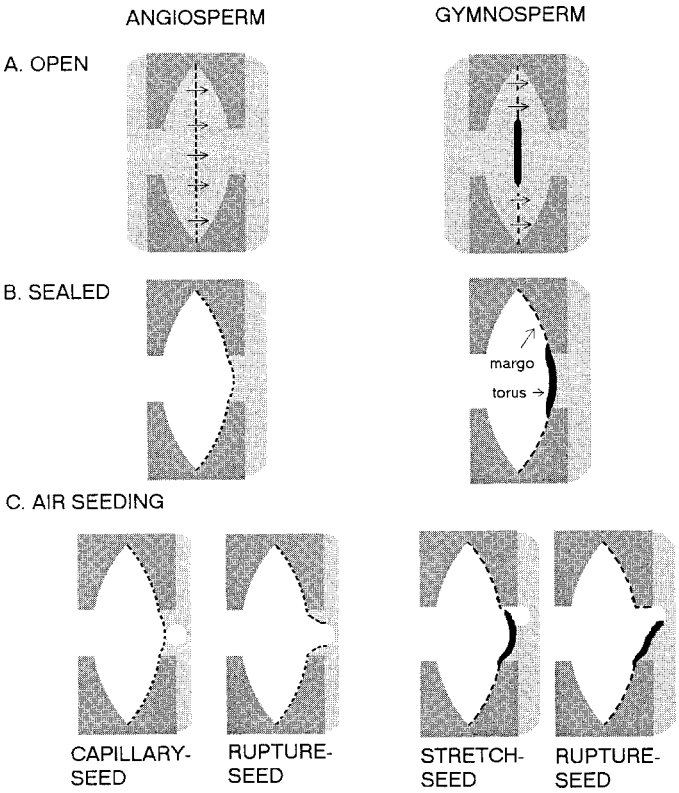

Fig. 1. Contrasting modes of interconduit pit function in angiosperm vessels (left) vs. gymnosperm tracheids with a torus-margo pit membrane (right). (A) Pits are open for water flow when surrounded by water. (B) Pits seal when an air–water meniscus is drawn into the membrane. Angiosperm pits seal by capillary forces in necessarily small membrane pores. Earlywood pits of gymnosperms seal by the aspiration of the essentially solid torus over the pit aperture after capillary forces at the margo pores have aspirated the membrane. (C) Air-seeding occurs when the pressure difference (P_a) between air (left) and water (right) across the pit membrane is high enough to force air through to nucleate cavitation. Vessel pits air-seed by capillary failure (''capillary-seeding'') if the air is sucked through preexisting pores in the pit membrane. Vessel pits ''rupture-seed'' if air is sucked through pores created by structural failure in the membrane. Torus-margo pits air-seed by ''stretch-seeding'' if the margo is elastically stretched to the aperture, exposing margo pores large enough to allow air passage. Pits rupture-seed if structural failure of the margo allows the torus to be pulled through the aperture.

to the same scrutiny. Tracheids, being single-celled, are limited in length to less than approximately 7 mm in tree species such as we examined. Shorter lumen length means that pit conductivity could become much more limiting for the overall tracheid conductivity. Is the torus-margo pit structure more efficient hydraulically than the homogenous pit membranes of angiosperms as suggested by Lancashire and Ennos (2002)? If so, it could compensate for shorter tracheid lengths. On the one hand, the much larger pores in the margo should increase membrane conductivity relative to the narrower pores of the angiosperm pit membrane. On the other hand, much of the membrane area is taken up by the nonconductive torus, and the pit aperture conductivity could be more important than the pit membrane for setting overall pit conductivity.

Another consideration is the role of tracheids in strengthening the axis—a role not required of vessels. This could require greater tracheid wall thickness than would be necessary just to resist implosion by negative pressure (Hacke et al., 2001a). Thicker walls would compromise conducting efficiency per conduit investment relative to the vessel network of angiosperms.

In this paper, we extend our previously described model (Sperry and Hacke, 2004) of xylem conduit function to gymnosperm tracheids with circular-bordered pit structure and torus-margo membranes. We employ a data set of 17 gymnosperm species (all conifers, except for one; Table 1) representing a wide range of air-seed pressure. We attempt to answer the following questions: (1) At the pit level, how does the torus-margo membrane compare with the angiosperm membrane in conductivity per air-seed pressure and per pit membrane area? (2) At the conduit level, how does the implosion resistance and hydraulic efficiency of tracheids compare with vessels? (3) How close does actual gymnosperm pit and tracheid structure come to achieving the maximum possible conducting efficiency?

MATERIALS AND METHODS

The data set—The data set (Table 1) on cavitation resistance and conduit anatomy included several species from previous studies (Hacke et al., 2001a) studied with methods described in the first paper (Sperry and Hacke, 2004). Cavitation resistance was represented by the air-seed pressure (P_a). This is the positive pressure difference required to force air into xylem conduits and cause cavitation. A species' air-seed pressure was the pressure required to cause a 50% loss of hydraulic conductivity by cavitation (the absolute value of P_{50} sensu Hacke et al., 2001a). By including species from numerous diverse habitats, we were able to obtain a wide range of P_a from a minimum of 0.8 MPa in *Taxodium distichum* roots to a maximum of 11.8 MPa in *Juniperus monosperma* stems (Table 1).

We included species from four families, including the sole nonconifer, *Ginkgo biloba*. In addition, we also sampled root and stem xylem from many species. By sampling broadly across phylogeny and organ, we intended to include all sources of variation in tracheid structure, so as to have the broadest comparative basis for evaluating structure–function relationships. We included roots for two reasons. First, they tend to be more vulnerable to cavitation than stems (Sperry and Ikeda, 1997; Linton et al., 1998; Kavanagh et al., 1999; Hacke et al., 2000) as seen in the present data set, in which root P_a averaged 2.2 MPa less than stem P_a for the nine species where data for both organs was available (Table 1). Second, tracheids in roots are in a very different mechanical environment than tracheids in stems, with potential consequences for their wall structure.

The anatomical measurements were made on the same or similar xylem samples used to determine the P_a. The hydraulic mean conduit diameter (D_c) was measured as described in the companion paper (Sperry and Hacke, 2004). The intertracheid wall thickness (t_w; Fig. 2C) was measured on tracheids with diameters within approximately 2 μm of D_c. The width of the intertracheid wall (b, Fig. 2A) was calculated as the side of a square with an area equal to the area of the tracheid lumen. For the rectangular shape of tracheids, this was a better approximation than setting $b = D_c$ as was done for the more circular geometry of vessels. Pit membrane (D_m), aperture (D_a), and torus diameters (D_t) were estimated for tracheids of diameter D_c. In gymnosperms, these values were strongly correlated with tracheid diameter. After establishing this correlation for each organ and species, the pit dimensions corresponding to tracheid diameter D_c were calculated from the correlation. Measuring the torus required staining with toluidine blue. In *Ginkgo biloba* and *Taxodium distichum*, the torus did not stain strongly and its diameter was not determined. Relevant tracheid and pit parameters are summarized in Fig. 2. Symbols are defined in Table 2.

APPLICATION OF CONDUIT MODEL TO TRACHEIDS

The model was the same that was described in detail for angiosperm vessels by Sperry and Hacke (2004). Here we provide only the central equations, adding detail when modifications were required to apply it to gymnosperm tracheids.

TABLE 1. Study species and air-seed pressure of gymnosperms listed alphabetically by family. Habitats are Wasatch Mountains of Utah (WM), Piedmont of North Carolina (NC), Utah's Great Basin (GB), greenhouse-grown plants (GH), Sonoran Desert (SD), University of Utah campus (UU), Georgia (GA), and northern California (CA). In some species both stem (S) and root (R) organs were measured. The air-seed pressure (P_a) is the absolute value of the negative pressure required to eliminate 50% of the hydraulic conductivity of the xylem sample. When two P_a values are given, the second one refers to roots. Source of P_a data is given when not obtained specifically for this paper.

Species	Family	Organ	Habitat	P_a (MPa)	Source for P_a data
Juniperus monosperma	Cupressaceae	S	SD	11.8	Pockman and Sperry, 2000
Juniperus osteosperma	Cupressaceae	S, R	WM	7.2, 5.5	Linton et al., 1998
Juniperus scopulorum	Cupressaceae	S, R	WM	7.3, 5.2	
Ginkgo biloba	Ginkgoaceae	S	UU	3.1	
Abies concolor	Pinaceae	S, R	WM	8.4, 3.4	
Abies lasiocarpa	Pinaceae	S, R	WM	3.3, 3.3	
Picea engelmannii	Pinaceae	S, R	WM	8.7, 5.0	
Pinus edulis	Pinaceae	S, R	GB	7.0, 4.2	
Pinus flexilis	Pinaceae	S	WM	5.1	
Pinus monophylla	Pinaceae	S	GB	6.3	
Pinus nigra	Pinaceae	S	GH	3.8	
Pinus palustris	Pinaceae	R	GA	2.3	
Pinus ponderosa	Pinaceae	S	GH	4.0	Hubbard et al., 2001
Pinus taeda	Pinaceae	S, R	NC	3.8, 1.1	Hacke et al., 2000
Pseudotsuga menziesii	Pinaceae	S, R	WM	4.8, 4.0	Sperry and Ikeda, 1997
Taxodium distichum	Taxodiaceae	S, R	NC	2.1, 0.8	
Sequoia sempervirens	Taxodiaceae	S	CA	3.4	

Conduit implosion pressure (P_i)—The bending stresses that arise when an air-filled tracheid abuts a water-filled one under negative pressure are greater than the hoop stresses encircling the conducting tracheid (Fig. 2A). As such, bending stresses pose the greater threat to the collapse of the water-filled conduit. The implosion pressure (P_i) was defined as the pressure difference across the tracheid wall required to cause the bending stress to exceed the wall strength. Presumably, the P_i is at least equal to the air-seed pressure (P_a) so that the safety factor from implosion (P_i/P_a) is one or more. A safety factor less than one would seem unlikely because wall collapse itself might trigger air-seeding.

The implosion pressure was calculated exactly as for angiosperm vessels:

$$P_i = (W/\beta)(t_w/b)^2 \, L_e \, (I_h/I_s) \quad (1)$$

where W is the strength of the solid wall material; and β is a coefficient that depends on the ratio of the conduit width (b) to conduit length (L) and was set to 0.25 for b/L of 0.5 or less (Young, 1989). The W was set to 80 MPa, the same as for angiosperm vessels (Hacke et al., 2001a).

The $(t_w/b)^2$ term is the ''thickness-to-span ratio,'' where t_w is the double wall thickness (Fig. 2C): the thicker the wall relative to its width, the greater the implosion pressure. The

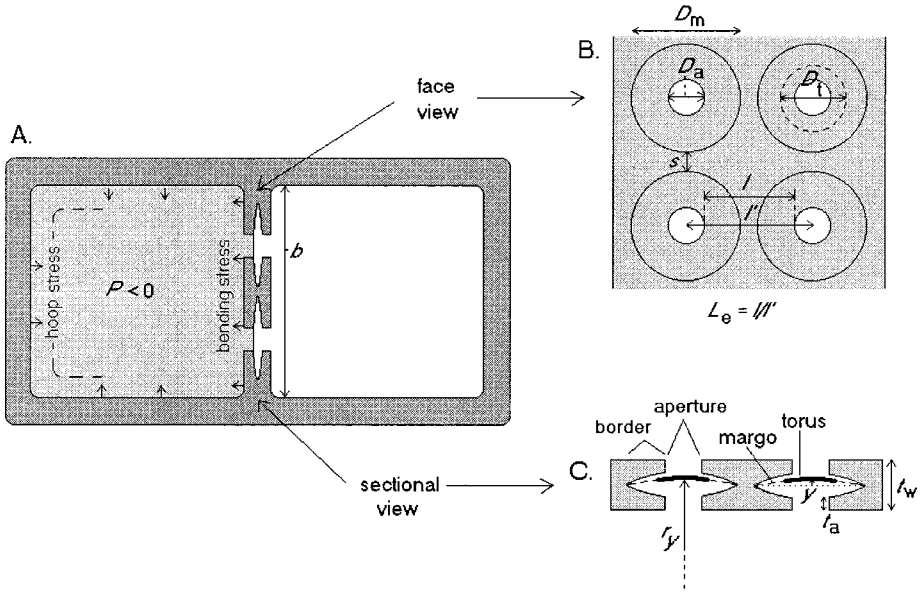

Fig. 2. Conduit wall structure. (A) Transverse view of two adjacent tracheids and pitted wall. Negative pressure in water-filled conduits (shaded) induces circumferential hoop stresses in the wall. Larger bending stresses are induced when the adjacent conduit is air-filled (nonshaded) and the common wall bends towards the water-filled side. b = width of the common wall. (B) Face view of pitted wall. D_a = aperture diameter; D_m = membrane diameter; D_t = torus diameter; s = spacing between pits; L_e = ligament efficiency (ratio of dimensions l/l′). (C) Transverse view of pitted wall showing pit aperture, border, and the torus-margo membrane: r_y = radius of curvature of membrane deflected distance y from flat position; t_w = double wall thickness; t_a = thickness of single aperture.

TABLE 2. List of parameters in the pit model with symbol, dimension (l, length; f, force; p, pressure [f · l^{-2}]; t, time), definition, and for constants, the values employed.

Symbol	Dimension	Definition
Constants		
A_f	l^2	cross-sectional area of microfibril spokes = 707 nm^2
a	degree	contact angle of air–water meniscus = 0°
E	f · l^{-2}	modulus of elasticity of microfibril spokes; default = 5 GPa
e_{ya}	—	spoke strain at aspiration (entire membrane) = 0.03
F	f · l^{-2}	strength of microfibril spokes; default = 2.2 GPa
s_f	l	spacing between parallel microfibrils in a sheet; default = 1.5 μm
t_f	l	thickness of microfibril strand = 30 nm
W	f · l^{-2}	strength of solid wall at saturation = 80 MPa
X	—	pitting coefficient; default = 2
υ	p·t	viscosity of water at 20°C = 0.001 Pa·s
τ	f · l^{-2}	surface tension of water at 20°C = 0.0728 N · m^{-1}
Input variables		
b	l	width of pitted wall between tracheids
D_c	l	mean hydraulic conduit diameter
D_a	l	pit aperture diameter
D_m	l	pit membrane diameter
D_t	l	torus diameter
L	l	conduit length
P_a	p	air-seed pressure = $-P_{50}$ sensu Hacke et al. (2001a)
t_w	l	thickness of double conduit wall (conduit of diameter D_c)
Output variables		
A_w	l^2	cross-sectional wall area of vessel
D_p	l	maximum pore diameter in relaxed membrane
D_p'	l	maximum pore diameter in stretched membrane
D_{pe}	l	equivalent pore diameter for membrane conductivity
e_y,	—	margo spoke strain at membrane displacement y
e_a, e_s	—	margo spoke strain at aspiration (e_a) and at stretch seeding (e_s)
h	—	fraction of membrane area occupied by pores
I_s	l^4	second moment of area for solid wall with no pit chambers present
I_h	l^4	second moment of area for median section through single pit
K_{sc}	l^2· t · p^{-1}	conduit conductivity per length and per wall area
K_{sp}	l · t · p^{-1}	pit conductivity per membrane area
n_s	—	number of radial microfibril spokes in membrane
n_{po}	—	number of pores in membrane
n_{pi}	—	number of pits in tracheid
n_{pi}'	—	number of pits in one row of opposite pitting
L_e	—	ligament efficiency
P_y	p	pressure across membrane at deflection y
P_c	p	capillary-seeding pressure
P_i	p	implosion pressure
R	p · t^{-1} · l^{-3}	hydraulic resistance
R_a	p · t^{-1} · l^{-3}	hydraulic resistance of single pit aperture
R_c	p · t^{-1} · l^{-3}	hydraulic resistance of tracheid
R_l	p · t^{-1} · l^{-3}	hydraulic resistance of tracheid lumen
R_m	p · t^{-1} · l^{-3}	hydraulic resistance of pit membrane
R_p	p · t^{-1} · l^{-3}	hydraulic resistance of pit
R_w	p · t^{-1} · l^{-3}	hydraulic resistance of pitted tracheid wall
r_y	l	radius of curvature of membrane at deflection y
s	l	distance between pit edges for opposite pitting arrangement
t_a	l	pit aperture length
y	l	deflection of membrane center from flat position

L_e is the ''ligament efficiency,'' which quantifies the spacing of the pit apertures in the wall. The L_e is equal to:

$$L_e = 1 - D_a/(D_m + s) \quad (2)$$

where s is the spacing between adjacent pit membranes (Fig. 2B). When pits were nearly as wide as the tracheid, s was taken as the distance between the pit membrane and the edge of the tracheid wall. The bigger the apertures relative to the pit membrane and the more closely the apertures are spaced, the lower the L_e and the weaker the wall. The (I_h/I_s) is the ''moment ratio.'' This ratio is the amount by which the second moment of area of a wall with pit chambers (I_h) is less than that for a solid wall perforated only by aperture-sized holes (I_s). To the extent that the hollowed-out chambers reduce the second moment of area, the wall will be weakened.

Air-seed pressure (P_a)—We considered three modes of air-seeding for conifer pit membranes with a torus-margo organization (Fig. 1): stretch-seeding and rupture-seeding as defined earlier (Fig. 1C); and also capillary-seeding through

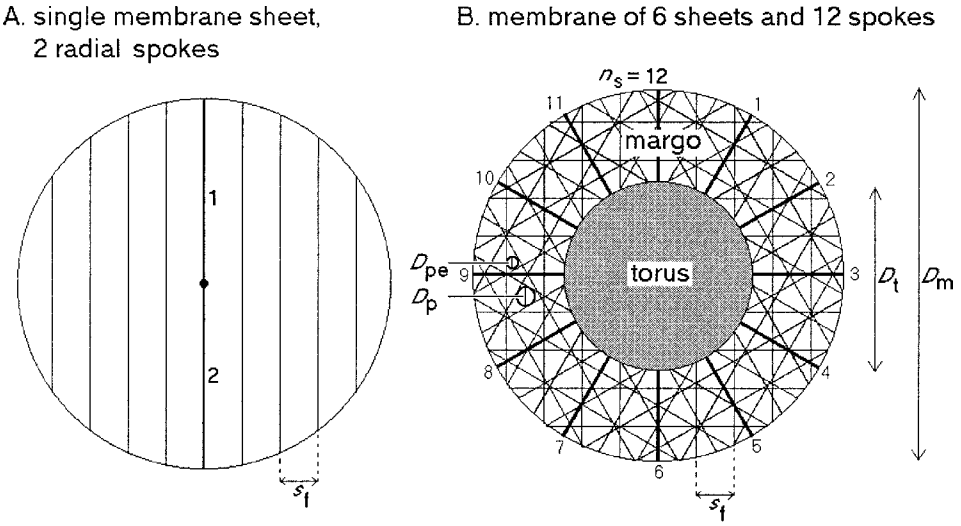

Fig. 3. Representation of pit membrane. (A) A single sheet of parallel microfibrils, each spaced distance s_f apart. One strand from each sheet formed a pair of radial spokes (numbered heavy line) assumed to bear the load on the stressed membrane. (B) A membrane composed of six sheets and n_s = 12 radial spokes (numbered heavy lines) overlaid with a nonporous and nonstretchable torus. D_p = maximum pore diameter; D_{pe} = equivalent pore diameter giving same membrane conductivity if all pores were of equal size; D_m = membrane diameter; D_t = torus diameter; s_f = spacing between strands of a single sheet.

pores in the margo prior to membrane aspiration (not shown in Fig. 1).

To predict the air-seed pressure, we calculated the pressure difference (P_y) required to deflect the membrane a progressively greater distance y from its unstressed flat position (Fig. 2C):

$$P_y = 2n_s E e_y A_f/(\pi D_m r_y) \quad (3)$$

where the subscript "y" denotes a value at displacement y, and r is the radius of curvature of the membrane (Fig. 2C). The n_s is the number of radial microfibril "spokes" assumed to bear the load on the membrane (Fig. 3), E is their elastic modulus, e_y is their strain (at y), and A_f their cross-sectional area (set to 707 nm^2 as for vessel pit membranes; Petty, 1972). When the membrane reached the pit chamber wall, aspiration occurred. The y at aspiration was calculated from an overall membrane strain (radial direction) at aspiration of 0.03, the same setting used for angiosperm pits.

For deflection beyond aspiration, Eq. 3 was modified to account for the deflection of the membrane through the pit aperture:

$$P_y = P_{asp} + 2n_s \Delta e_y E A_f/(\pi r_y D_a) \quad (4)$$

where P_{asp} is the pressure causing aspiration, D_a is the aperture diameter, r is the radius of curvature of the membrane deflecting through the aperture, and Δe is the additional strain caused by deflection through the aperture.

Equations 3 and 4 were the same as those used for vessel pits with the exception that for conifer pits, the membrane strain was assumed to occur only within the thinner and presumably more extensible margo portion of the membrane. Thus, for an entire membrane strain (torus + margo) at aspiration of 0.03, the margo spoke strain at aspiration (e_a) would be:

$$e_a = 0.03\ D_m/(D_m - D_t) \quad (5)$$

Air-seeding occurred when the P_y reached either the capillary-seed pressure, rupture-seed pressure, or stretch-seed pressure. Whichever of these three limiting pressures was lowest determined the mode of air-seeding. The capillary-seed pressure (P_c) was

$$P_c = 4\tau\cos(a)/D_p' \quad (6)$$

where τ is the surface tension of water, a is the contact angle between meniscus and wall, and D_p' is the *stretched* diameter of the membrane pores. The D_p' was calculated assuming for simplicity's sake that microfibril strands did not become thinner as the membrane deflected. The rupture-seed pressure was equal to the P_y where spoke stress (Ee_y/A_f) equaled the spoke strength (F). The stretch-seed pressure was the P_y where the margo strain was sufficient to expose the margo pores at the pit aperture. The margo spoke strain at stretch-seeding (e_s) was:

$$e_s = (D_t - D_a + 0.03D_m)/(D_m - D_t). \quad (7)$$

Stretch-seeding also required that the exposed margo pores be large enough to capillary-seed.

Membrane structure—The structure of the torus-margo membrane was represented in the same way as the vessel pit membrane, except that a torus was present (Fig. 3). The membrane was composed of $n_s/2$ microfibril sheets superimposed on one another, with the microfibrils of each sheet spaced a constant distance s_f apart. For such a membrane, the diameter of the largest circular pore (D_p) inscribed between microfibrils (Fig. 3B) was approximately:

$$D_p \approx 2s_f \sin[180/(n_s + 2)]. \quad (8)$$

Petty's (1972) measurements of D_p and n_s give an s_f of approximately 1.5 μm, which was used as the default value for both conifer and angiosperm membranes. As noted in the results section, we assessed the effect of varying the s_f setting from the default over a range from 0.5 to 3.0 μm.

To match a given membrane structure with a specific air-seed pressure, we increased the number of spokes (n_s) by increments of two (two spokes per microfibril sheet), and calculated the air-seed pressure for each spoke setting until the desired air-seed pressure was reached.

Pit and conduit hydraulic conductivity—The hydraulic resistance of the pit membrane (R_m) was:

$$R_m = [24\upsilon/(n_{po}D_{pe}^3)]f(h) \quad (9)$$

where n_{po} is the number of pores in the membrane, υ is the viscosity of water, and f(h) is a function of the fraction of the membrane area occupied by pores (h), which accounts for the effect of pore spacing on pore conductivity (Tio and Sadhal, 1994). The D_{pe} was the equivalent pore diameter (Fig. 3B) that gave the same membrane conductivity for the same number of pores as in the actual membrane. The equivalent pore diameter was approximately 63% of D_p. The pore number (n_{po}) was estimated from the total membrane area divided by the area of a single circular pore (of diameter D_{pe}), including the surrounding microfibril strand.

The hydraulic resistance of the pit aperture (R_a) was (Dagan et al., 1982):

$$R_a = 128t_a\upsilon/(\pi D_a^4) + 24\upsilon/D_a^3 \quad (10)$$

where t_a is the length of one aperture (Fig. 2C). The t_a was calculated from the double wall thickness (t_w) and depth of the pit chamber. The total pit resistance (R_p) was equal to R_a and R_m in series: $R_p = R_a + R_m$. We expressed the pit resistance as a conductivity per membrane area (pit K_{sp}).

The total tracheid resistance (R_c) was computed from the lumen resistance (R_l) and the pit resistance (R_w) in series ($R_c = R_w + R_l$) according to Lancashire and Ennos (2002). This calculation assumes that water on average traverses just half of a conduit's total length. The lumen resistance is estimated as half of the Hagen-Poiseuille resistance for a tracheid of length L:

$$R_l = 64\upsilon L/(\pi D_c^4). \quad (11)$$

The pit resistance is the resistance of just half of the tracheid's pits:

$$R_w = 2R_p/n_{pi} \quad (12)$$

where n_{pi} is the number of pits per tracheid. This was given by

$$n_{pi} = \text{int}[LX/(D_m + s)]\ n_{pi}' \quad (13)$$

where int[number] returns the largest integer of the number, s is the minimum horizontal or vertical distance between pit edges (Fig. 2B), and LX is the cumulative length of pitted walls, with the ''pitting coefficient'' X being the proportionality factor between the tracheid length (L) and the cumulative pitted length. For example, if a tracheid had pitted walls on two sides for all of its length, $X = 2$. The n_{pi}' is the number of pits (an integer) fitting side-by-side across the conduit wall of width b in an opposite pitting arrangement (Fig. 2). The n_{pi}' was usually 1 for tracheids in stems, but could be higher in roots. Tracheid length (L) and pitting coefficient (X) were not measured, and we present a sensitivity analysis of these variables in the results.

To express the hydraulic efficiency of a conduit, we converted R_c to the hydraulic conductivity of a single tracheid on a per conduit length and per unit cross-sectional wall area basis (vessel K_{sc}):

$$K_{sc} = L/(R_c A_w) \quad (14)$$

where A_w is the cross-sectional area of the conduit wall. To account for the wall investment in the conduit over its entire length, the A_w was calculated from the total wall volume of the conduit (V) divided by the conduit length ($A_w = V/L$). Volume calculations were identical to those used for angiosperm vessels.

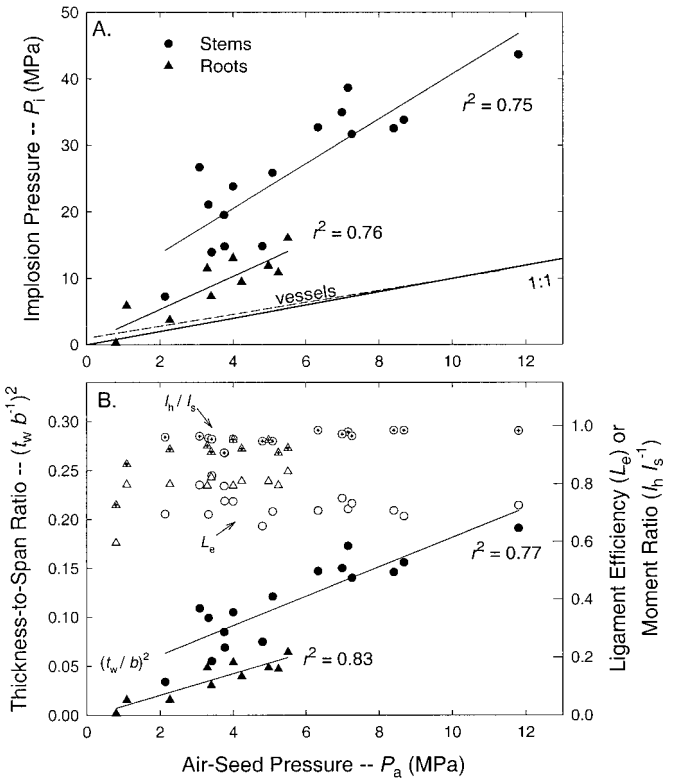

Fig. 4. (A) Implosion pressure (P_i) vs. air-seed pressure (P_a) for stem (circles) and root (triangles) tracheids. Lowest solid line is 1 : 1; dashed line is for vessels (from Sperry and Hacke, 2004). (B) Components of implosion pressure vs. air-seed pressure. Left ordinate and solid symbols (circles = stems; triangles = roots) are the thickness-to-span ratios $(t_w/b)^2$. Right ordinate is the ligament efficiency (L_e; open circles for stems, triangles for roots) or the moment ratio (I_h/I_s; dotted circles stems, dotted triangles for roots).

RESULTS

Wall implosion pressure (P_i) and tracheid dimensions—The predicted implosion pressure exceeded the air-seed pressure across the full range (Fig. 4A). The two pressures were tightly correlated, but with different intercepts in root vs. stem tracheids. Root tracheids had an intercept no different than zero, implying a constant safety factor from implosion (P_i/P_a), which averaged 2.4 ± 0.3. Stem tracheids had a substantially positive intercept of 8.1 MPa, indicating additional wall reinforcement that was independent of air-seed pressure. The average safety factor for stem tracheids was 4.8 ± 0.4, double that in roots. Tracheids from both stems and roots had higher safety factors against implosion than angiosperm vessels as reported in the first paper (Fig. 4A, dashed ''vessel'' line).

The increase in implosion pressure with air-seed pressure was entirely the result of increased thickness-to-span ratio $(t_w/b)^2$ (Fig. 4B, solid symbols). The ligament efficiency (L_e) did not increase with air-seed pressure, remaining constant at 0.75 ± 0.01 (Fig. 4B, open symbols). The spacing between pits or between pits and the edge of the tracheid (Fig. 2B; s) was generally negligible, meaning the L_e was chiefly a function of the diameter of the pit aperture and membrane ($L_e \approx 1 - D_a/$

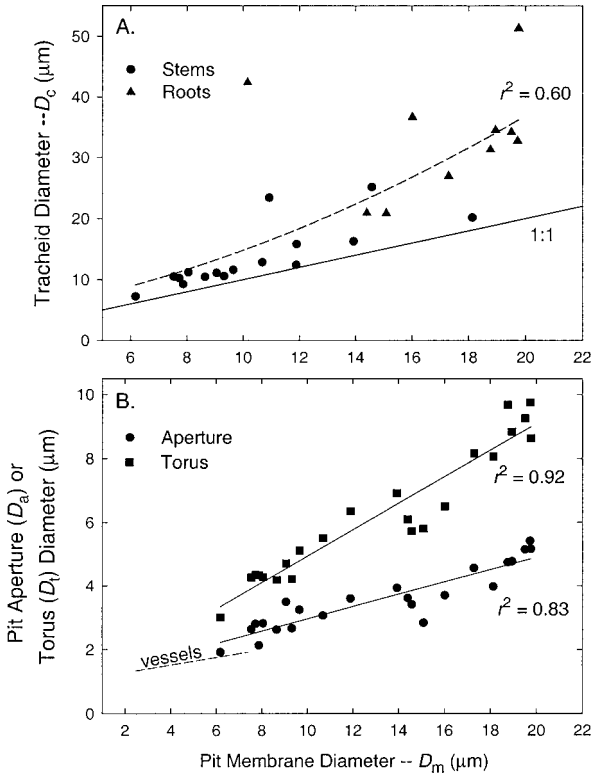

Fig. 5. (A) Hydraulic mean tracheid diameter (D_c) vs. pit membrane diameter (D_m) for stem (circles) and root (triangles) tracheids. Curve is a quadratic fit to pooled data ($r^2 = 0.60$). (B) Pit aperture diameter (D_a; circles) or torus diameter (D_t; squares) vs. pit membrane diameter (D_m) for pooled root and stem tracheid data. Dashed line shows linear correlation for vessels from Sperry and Hacke (2004).

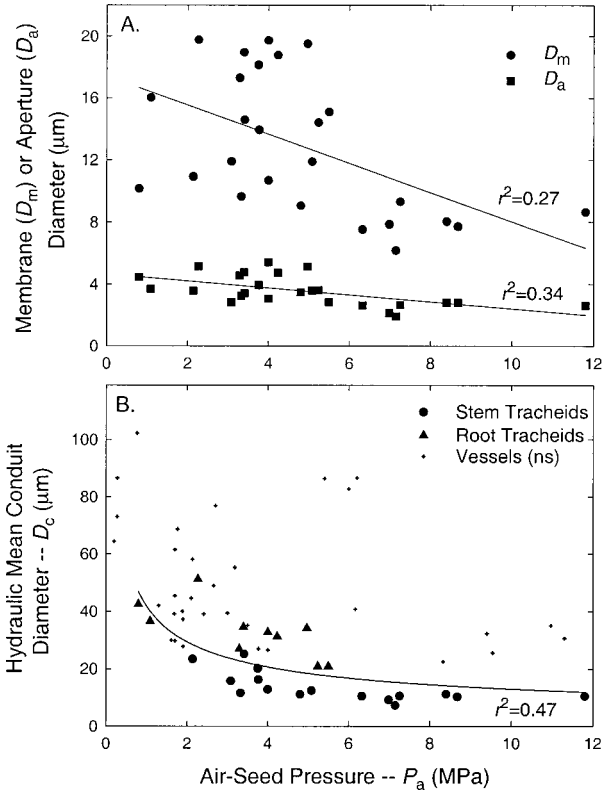

Fig. 6. (A) Pit membrane (D_m; circles) or pit aperture (D_a; squares) diameter vs. air-seed pressure (P_a) for pooled root and stem tracheids. (B) Hydraulic mean conduit diameter (D_c) vs. air-seed pressure (P_a) for root (triangles) and stem (circles) tracheids from the data set ($r^2 = 0.47$ for pooled data, fit by a two-parameter power function). Crosses show vessel data from Sperry and Hacke (2004).

D_m). The moment ratio (I_h/I_s) did not change with air-seed pressure and averaged 0.94 ± 0.01 (Fig. 4B, dotted symbols). Thus, the presence of pits lowered the implosion pressure by about 30% relative to a solid wall of the same dimensions, with apertures causing 25% and chambers causing 5% of the effect.

Tracheid pits were essentially as wide as the tracheid up to tracheid diameters of approximately 20 μm (Fig. 5A) and greatly exceeded the diameter range reported in the first paper for vessel pits (Fig. 5B, dashed line). The D_a was correlated with D_m (Fig. 5B, circles), keeping L_e relatively constant with pit size. The torus diameter also increased linearly with pit membrane size (Fig. 5B, squares), staying at about 49% of the pit diameter.

Tracheid pit membranes and apertures were significantly smaller in diameter for greater air-seed pressures (Fig. 6A). This was consistent with a decline in tracheid diameter with air-seed pressure (Fig. 6B) and the fact that pit membrane and tracheid diameter were correlated (Fig. 5A).

The scaling relationships in Figs. 4–6 allowed us to define what we hereafter refer to as the ''average'' tracheid for the data set. The average tracheid had the mean $P_a = 4.8$ MPa for the data set, which corresponded to a mean hydraulic diameter of $D_c = 19$ μm from the curve fit in Fig. 6B, a $D_m = 12.9$ μm and $D_a = 3.6$ μm from the correlations in 6A, and $D_t = 6.15$ from the correlation in Fig. 5B. The corresponding thickness-to-span ratio (hence setting the t_w) was 0.1 from the stem tracheid regression Fig. 4B.

Mode of air-seeding and the mechanical properties of membrane microfibrils (E, F)—As shown for vessel pits in the first paper (Sperry and Hacke, 2004), the mode of air-seeding depended on the settings for membrane spoke strength (F) and elastic modulus (E; Fig. 7). The actual values for these properties are ambiguous, conceivably ranging from theoretical values for cellulose microfibrils to experimental values for primary cell walls ($F = 25$ to $F < 1$ GPa; $E = 250$ to $E < 3$ GPa; (Mark, 1967; Petty, 1972; Jeronimidis, 1980; Ashby et al., 1995; Hepworth and Vincent, 1998a, b). A sensitivity analysis predicted four types of pit function depending on the F and E settings (Fig. 7).

Type 1 pits showed aspiration and stretch-seeding. These pits had high F and low E—strong, flexible membranes (Fig. 7, upper left).

Type 2 pits showed no aspiration and capillary-seeding through margo pores. These were associated with high F and high E—strong, stiff membranes. These pits occurred for F and E outside of the range shown in Fig. 7.

Type 3 pits showed no aspiration and rupture-seeding. These were associated with relatively low F and high E—weak, stiff membranes (Fig. 7, lower right).

Type 4 pits showed aspiration and rupture-seeding. These pits occupied a wedge between type 1 and 3 pits (Fig. 7).

The aspiration boundary between types 3 and 4 (Fig. 7, dashed diagonal) is the F/E ratio that equals the margo strain at aspiration (e_a) because no pit can aspirate if in doing so it

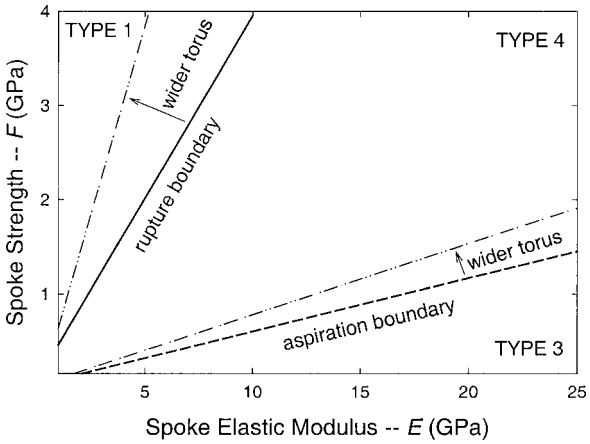

Fig. 7. Influence of microfibril spoke strength (F) and elastic modulus (E) on pit aspiration and mode of air-seeding for the average tracheid as defined in text. Type 1 pits stretch-seeded after aspiration. Type 3 pits rupture-seeded without aspiration. Type 4 pits rupture-seeded after aspiration. Not shown are type 2 pits that capillary-seeded without aspirating. The solid ''rupture boundary'' divides rupture-seed pits (below) from capillary-seed pits (above). The dashed ''aspiration boundary'' divides aspirating pits (above and to left) from nonaspirating pits (below and to right). Increasing the torus diameter relative to the rest of the pit caused the rupture and aspiration boundaries to steepen (dash-dotted lines for D_t = 60% of D_m vs. normal 49%) and vice versa.

must stretch past the rupture point. The margo strain at aspiration depends on the torus diameter relative to the membrane diameter (Eq. 5). For a torus diameter 49% of the pit diameter (Fig. 5B), the margo strain at aspiration was approximately 0.06, which also gives the slope of the aspiration boundary. Increasing the torus diameter relative to the pit membrane diameter resulted in a higher margo strain at aspiration and a steeper slope for the aspiration boundary (Fig. 7, dash-dotted line above aspiration boundary for D_t = 60% of D_m).

The rupture boundary between pit types 1 and 4 (Fig. 7, solid diagonal) is the F/E ratio that equals the margo strain at stretch-seeding (e_s) because no pit can stretch-seed if to do so it must stretch beyond the rupture point. The margo strain at stretch-seeding depends on the torus and aperture diameters relative to the membrane diameter (Eq. 7). The aperture diameter averaged 29% of the pit membrane diameter (Fig. 5B), which together with the scaling of the torus gives an approximate margo strain at stretch-seeding of 0.45, which was just steeper than the slope of the rupture boundary (Fig. 7; slope = 0.40). Increasing the torus diameter relative to pit membrane and aperture diameters caused a higher margo strain at stretch-seeding and a steeper rupture boundary (Fig. 7, dash-dotted line above rupture boundary for D_t = 60% of D_m).

The boundaries between pit types 1, 3, and 4 for the F and E range shown in Fig. 7 were essentially independent of the air-seed pressure and microfibril spacing (s_f) because neither of these influenced the margo strain at aspiration or at stretch-seeding. The boundaries were also insensitive to changes in pit size as long as the torus and aperture diameters scaled with pit membrane diameters as observed (Fig. 5B). This suggests that the observed scaling of pit dimensions may be necessary to maintain the same mode of air-seeding across a range of pit sizes.

If we assume that pits do aspirate as has been observed (Petty, 1972) and that they do not rupture-seed—because this would cause irreversible damage to the membrane—we can

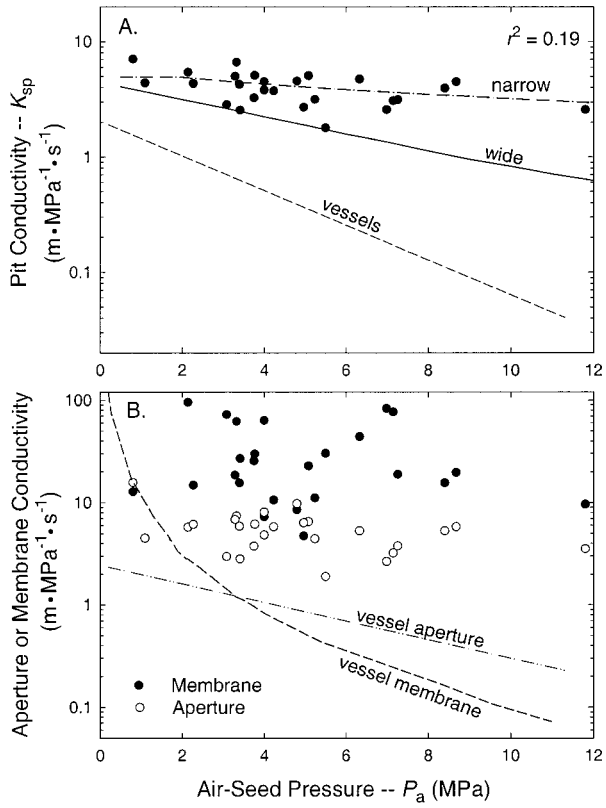

Fig. 8. (A) Pit conductivity per membrane area (pit K_{sp}) vs. air-seed pressure (P_a) for root and stem xylem samples in the data set (symbols; overall r^2 = 0.19). Dash-dotted line is for tracheids of the narrowest diameter in the data set (D_c = 7.3 μm; D_m = 6.2; D_a = 1.9; D_t = 3.0 μm). Solid line is for tracheids of the widest diameter (D_c = 51 μm; D_m = 19.8; D_a = 4.8; D_t = 9.0 μm). Dashed line is correlation for vessel data from Sperry and Hacke (2004). (B) Aperture (open symbols) or membrane (solid symbols) conductivity per membrane area vs. air-seed pressure for same xylem samples from (A). Dotted line shows vessel aperture conductivites and dashed line shows vessel membrane conductivities from Sperry and Hacke (2004).

narrow down the range of F and E values for the microfibril spokes to what results in type 1 pits (Fig. 7). For pits of average torus proportions, the F/E must exceed approximately 0.40. Except where noted, the default setting for all subsequent analyses was F = 2.2 and E = 5 GPa, which insured type 1 pits for observed pit dimensions. These settings are intentionally the same that we used for the membrane spokes of vessel pits in the first paper of this series (Sperry and Hacke, 2004).

Pit conductivity (pit K_{sp}) vs. air-seed pressure (P_a)—There was a slight, but significant decline in tracheid pit K_{sp} with increasing P_a (Fig. 8A, r^2 = 0.19). Pit K_{sp} dropped by a factor of 1.7 for a 10-fold increase in P_a from 1 to 10 MPa. These calculations were for pits and tracheids of measured diameters and of a wall thickness giving the P_i predicted from the root and stem regressions in Fig. 4A.

The decline in tracheid pit K_{sp} was considerably less than the 30-fold decline we found for vessel pit K_{sp} over the same 1–10 MPa P_a range in the companion paper (Sperry and Hacke, 2004) (Fig. 8A, dashed line). In addition, conifer pit K_{sp} was considerably greater than vessel K_{sp}—by a factor of 3.3 at P_a = 1 MPa, increasing to a factor of 43 at P_a = 10 MPa.

Torus-margo pit K_{sp} was limited by aperture conductivity

rather than membrane conductivity, because the former was consistently less than the latter across the P_a range (Fig. 8B, compare open vs. solid symbols). The decline in tracheid pit K_{sp} with P_a was attributable to a statistically nonsignificant trend for decreasing membrane conductivity and aperture conductivity with P_a (Fig. 8B). Membrane conductivity tended to decline because of the higher number of microfibril spokes (and hence smaller margo pores) required to hold the membrane against greater pressures. Aperture conductivity tended to decline because of the thicker walls (and hence larger aperture depth t_a) required to keep P_i equal to P_a and because of the decline in aperture diameter with increasing P_a (Fig. 6A).

In contrast, the vessel analysis in the companion paper (Sperry and Hacke, 2004) showed that vessel pits were generally membrane-limited except at low P_a (Fig. 8B, compare vessel aperture vs. membrane lines). The steeper decline in vessel pit K_{sp} with air-seed pressure was primarily a result of a much more pronounced decline in membrane conductivity compared with the torus-margo pit membrane. The low membrane conductivity of the intervessel pit was the main reason why vessel pits analyzed in the first paper had a much lower K_{sp} than tracheid pits. In addition, vessel pits had a slightly narrower aperture diameter for a given pit membrane diameter than tracheid pits (Fig. 5B), causing the vessel pit aperture conductivity to be lower in vessels vs. tracheids (Fig. 8B).

The scatter in the relationship between tracheid pit K_{sp} with P_a was related to variation in tracheid and pit membrane size. Narrower tracheids had narrower pit membranes (Fig. 5A) and also greater pit K_{sp} than wider tracheids (Fig. 8A, narrow line vs. wide line). The greater hydraulic conductivity of pits in narrow tracheids was due to both higher membrane conductivity and aperture conductivity. Membrane conductivity was higher in pits of narrow tracheids because the smaller pit membranes required fewer spokes to support the same air-seed pressure vs. wide pit membranes. Fewer spokes translated into larger margo pores and higher conductivity. The large variation in membrane conductivity (Fig. 8B, solid symbols) was attributable to variation in pit membrane diameter. Aperture conductivity was higher in pits of narrow tracheids because the wall thickness was less for the same thickness-to-span ratio compared to the walls of wide tracheids. The variation in aperture conductivity (Fig. 8B, open symbols) was thus linked to variation in wall thickness with tracheid diameter.

The tight scaling of torus diameter with membrane and aperture diameter (Fig. 5A) was consistent with the torus size required to maximize the pit K_{sp} (Fig. 9). We defined the ''torus overlap'' as the fraction of the pit border width that was covered by the torus $[(D_t - D_a)/(D_m - D_a)]$. The scaling in Fig. 5B corresponded with a torus overlap between 0.21 and 0.38 (Fig. 9, horizontal bar above abscissa). This narrow range of overlap corresponded with values that maximized the calculated pit K_{sp} when the torus diameter was varied while keeping D_m and D_a constant at the observed ratio (Fig. 9). Although a torus narrower than the optimum allowed for greater margo area, it also reduced the amount the margo stretched before air-seeding. Thus, to maintain an air-seed pressure, more margo spokes were required, which reduced membrane pore size and conductivity. A torus wider than the optimum reduced the margo area, countering the advantage of larger margo pore size. A wider torus also led to rupture-seeding, because the margo could not be stretched to the aperture without exceeding its point of failure. Rupture-seeding occurred at an overlap of between 0.31 and 0.34 for the default settings of F (2.2 GPa) and E (5.0 GPa; Fig. 9, vertical dash-dotted line). The optimal torus overlap was insensitive to pit size (not shown), but became much broader at low air-seed pressure (Fig. 9, compare average P_a = 4.8 MPa with P_a = 1.0 MPa). The optimum also increased slightly with large increases in the F/E ratio (not shown).

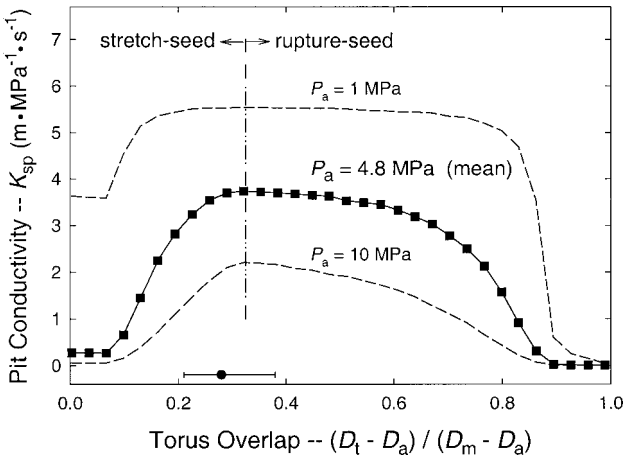

Fig. 9. Pit conductivity per membrane area (K_{sp}) vs. torus overlap $[(D_t - D_a)/(D_m - D_a)]$ for the average tracheid as defined in text. The line with symbols is for the average air-seed pressure (P_a = 4.8 MPa). The upper dashed curve is for a P_a of 1.0 MPa near the minimum, and the lower dashed curve is for a P_a of 10 MPa near the maximum. Regardless of air-seed pressure, maximum pit K_s occurred for a torus overlap of between 0.24 and 0.30—within the observed range (horizontal bar above abcissa; mean and range). Rupture-seeding (vertical dashed line) occurred for an overlap of between 0.31 and 0.34 for the default settings of F = 2.2 GPa, E = 5 GPa.

Tracheid conductivity (K_{sc}) vs. air-seed pressure—The tracheid K_{sc} incorporated both the pit and lumen components of the overall tracheid conductivity. It was expressed per conduit length and per wall area allocated to conduit construction. A greater tracheid K_{sc} means the plant can move more water with less drop in water potential per unit length and less investment in wall material per unit length.

As was shown for vessel K_{sc} in the companion paper (Sperry and Hacke, 2004), the tracheid K_{sc} increased in sigmoidal fashion with increasing tracheid length (L; Fig. 10). Tracheid lengths were not measured, and the curves in Fig. 10 are for the average tracheid in the data set as a function of increasing L. All other dimensions equal, a short tracheid has low conductivity because it is limited by the low conductivity of the pitted tracheid walls (Fig. 10, pit-limited). Lengthening the same tracheid causes the conductivity to increase as the relatively high conductivity of the lumen becomes significant. When long enough, the tracheid achieves a maximum ''saturated'' conductivity that is limited by the lumen diameter and conduit wall area (Fig. 10, lumen-limited). This saturated conductivity was calculated directly by the model, but a summary equation indicates its dependency on tracheid size and wall thickness:

$$\text{saturated conduit } K_{sc} \propto D_c^4/[(t_w + D_c)^2 - D_c^2] \qquad (15)$$

where the proportionality depends in part on how much of the wall is occupied by pits.

The ''saturating length'' is the tracheid length required to achieve 95% of the saturated tracheid K_{sc}. It may represent the optimal tracheid length: shorter tracheids cost the plant con-

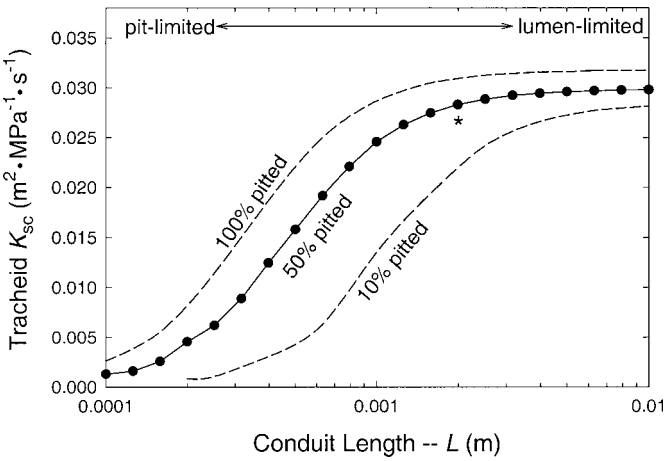

Fig. 10. Tracheid K_{sc} vs. tracheid length (L) for average tracheids as defined in text. Symbols represent the default setting for pits on 50% of the tracheid wall. Dashed lines indicate 10% and 100% pitting as indicated. Short tracheids were limited by pit conductivity and had low K_{sc}; longer tracheids were limited by lumen conductivity and had a maximum saturated K_{sc} given by Eq. 15. The ''saturating length'' (asterisked point at $L = 0.002$ m) was defined as the tracheid length required to achieve 95% of the saturated tracheid K_{sc}.

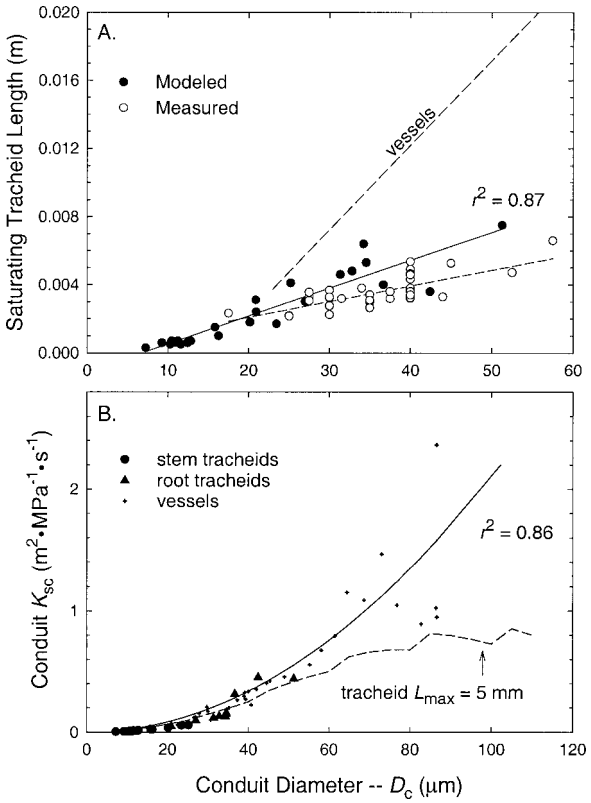

Fig. 11. (A) Saturating conduit length vs. conduit diameter for pooled stem and root samples from the data set (solid circles; $r^2 = 0.87$; 50% pitting). Open circles are literature values for average tracheid lengths and diameters of 37 softwoods (open symbols, Panshin and de Zeeuw, 1970, tables 4–4, 4–5). Dashed line is correlation for vessel data from Sperry and Hacke (2004) (50% pitting). (B) Conduit K_{sc} vs. conduit diameter (D_c) for stem (circles) and root (triangles) tracheids from the data set. Vessel data from Sperry and Hacke (2004) shown as crosses. Solid curve is best fit to pooled vessel and tracheid data ($r^2 = 0.84$) based on Eq. 15. Dashed line is for tracheids with length capped at a maximum of $L = 5$ mm. For this calculation, the pit dimensions followed the scaling relationships between D_c, D_m, D_t, and D_a shown in Fig. 5 but were extrapolated beyond the maximum observed D_c of 51 μm.

ductivity, and longer tracheids provide little benefit in conductivity when water-filled, yet cause a greater drop in conductivity when embolized.

The saturating tracheid length decreased with increasing length of pitted wall (LX; Eq. 13): the fewer pits, the more limiting was the pit conductivity and hence the longer the tracheid must be to reach its saturated conductivity. The saturated tracheid length increased from 1.3 mm when all sides of the tracheid were completely pitted (Fig. 10; 100% pitting, $X = 4$) to 4.6 mm when only 10% of the wall space was pitted (Fig. 10; 10% pitting, $X = 0.4$). Tracheids are generally pitted only on their radial walls. Assuming the two radial walls were completely pitted and the two tangential walls were not pitted, we adopted a pitting percentage of 50% ($X = 2$) as the default for subsequent analysis. This also matched the default used in the vessel analysis in the companion paper (Sperry and Hacke, 2004). A 50% pitting percentage yielded a saturating tracheid length of 2 mm (Fig. 10, asterisk by 50% pitting curve).

The saturating length also depended on tracheid diameter. The wider the tracheid, the less limiting the lumen conductivity compared to the pit conductivity, and the longer the lumen must be to achieve the maximum tracheid K_{sc}. The saturating lengths predicted for tracheids in the data set (50% pitting) agreed well with length vs. diameter data from a literature data set of 37 species (Fig. 11A, compare solid vs. open symbols; data from Panshin and de Zeeuw, 1970, tables 4–4, 4–5). Maximum average tracheid length in the literature data set for conifers was 5.6 mm, with a maximum average diameter of 56 μm.

Compared to vessels, tracheids had a much shorter saturating length (Fig. 11A, compare dashed vessel line with modeled symbols). The shorter saturating length of tracheids was because of their considerably greater pit K_{sp} compared with vessels (Fig. 8A). A higher pit conductivity for tracheids means the tracheid lumen does not have to be as long to limit the conduit conductivity.

Assuming that tracheid length was equal to the saturating length and that tracheids were 50% pitted, we predicted the relationship between tracheid K_{sc} and tracheid diameter (Fig. 11B). Tracheid K_{sc} increased as a power function in accordance with Eq. 15. The scatter was due to variation in air-seed pressure (and hence t_w in Eq. 15) that was independent of conduit diameter. Notably, tracheids and vessels were predicted to be similar in their K_{sc} (Fig. 11B, compare symbols with crosses)—the only difference was attributable to variation in t_w, depending on the safety factors from conduit implosion (Fig. 4A). Although tracheids are usually considered to be inherently less efficient than vessels, the model suggests that this is not true if both conduits are at their saturating lengths and they have equal pitting volumes and thickness-to-span ratios.

Tracheids did become less efficient than vessels when the tracheid diameter was increased while holding tracheid length constant at the near maximum obtained from the literature data set ($L = 5.0$ mm). At large diameters, tracheid K_{sc} plateaued at an approximately constant value (Fig. 11B, dashed line). Any advantage of increased lumen diameter was offset by the limitation of pit conductivity as wider tracheids became too short to achieve the saturated K_{sc}.

Continuing to assume tracheids at their saturating length, we predicted the relationship between tracheid K_{sc} and air-seed

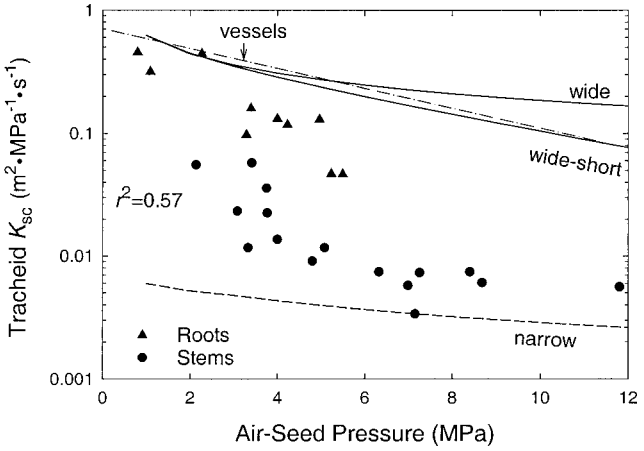

Fig. 12. Tracheid K_{sc} vs. air-seed pressure (P_a) for stem (circles) and root (triangles) xylem samples in the data set ($r^2 = 0.57$ for linear correlation of pooled data). The tracheids were at their saturating length. The dash-dotted ''vessel'' line is the correlation for vessel data from Sperry and Hacke (2004). Solid ''wide'' line is for maximum tracheid diameter in the data set (D_c = 51 μm) with its pit dimensions held constant (D_m = 19.8; D_a = 5.2; D_t = 8.6 μm) and L at the saturating length. Solid ''wide-short'' line is the same, except L was capped at a maximum of 5 mm. Dashed ''narrow'' line is for the minimum tracheid diameter in the data set (D_c = 7.2 μm) with its pit dimensions held constant (D_m = 6.2; D_a = 1.9; D_t = 3.0 μm) and L of the saturating length.

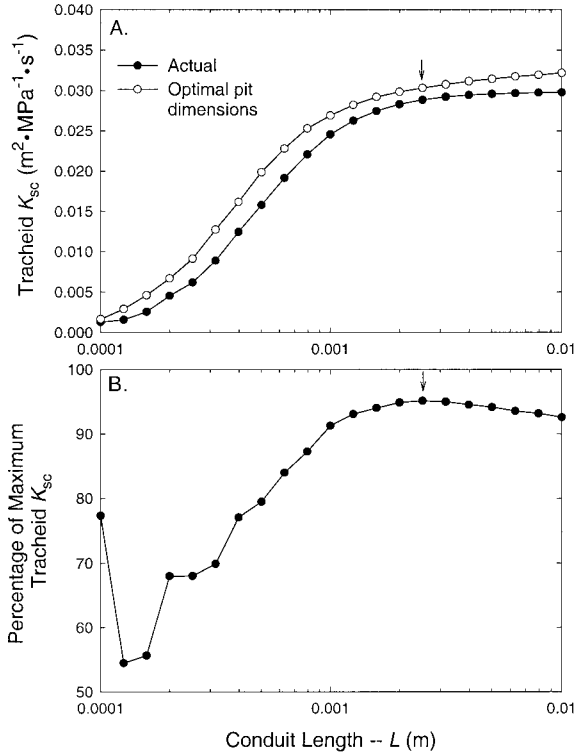

Fig. 13. (A) Tracheid K_{sc} vs. tracheid length (L). ''Actual'' values (solid symbols) are from Fig. 10 for average tracheids from the data set with 50% pitting. Open symbols show the maximum possible K_{sc} achieved by allowing pit dimensions (D_m, D_a, D_t) to vary for each length setting. (B) The percentage of the maximum possible K_{sc} achieved by actual tracheids for each length (L). Actual K_{sc} achieved 95% of the maximum (arrows in panels B and A) near the saturating tracheid length.

pressure (Fig. 12). There was a significant negative relationship between this tracheid K_{sc} and increasing air-seed pressure ($r^2 = 0.57$). The scatter was related to independent variation in tracheid diameter. Wider tracheids had much higher tracheid K_{sc} than narrow ones (Fig. 12, compare wide vs. narrow lines) as expected from Eq. 15 for saturated K_{sc}. Although the pits in wide conduits are *less* conductive due to greater wall thickness (Fig. 8A), in long tracheids where pit conductivity is not limiting this disadvantage is masked by the much greater conductivity of a wide lumen. The decline in tracheid K_{sc} for constant tracheid diameter (e.g., wide and narrow lines) was due to increasing wall thickness required to maintain the necessary implosion pressure as air-seed pressure increased.

Tracheids were less conductive than vessels, especially at high P_a (Fig. 12, compare symbols with dashed ''vessel'' line). However, as pointed out before, this was not because tracheids were inherently less efficient than vessels of the same diameter and P_a. Instead, it was because tracheids were generally much narrower than vessels (Fig. 6A). The largest tracheid was 51 μm in diameter (*Pinus palustris* roots), which approximated the average vessel diameter in the angiosperm data set (49 μm). When the tracheid K_{sc} was calculated for 51 μm diameter across all P_a (Fig. 12, solid wide line), it approximated or even exceeded the vessel K_{sc}—indicating that the only factor preventing tracheids from achieving a higher K_{sc} was maintaining a wider diameter.

One explanation for the lack of wide tracheids at high P_a is that they cannot achieve their saturating length (and maximum K_{sc}) because of the higher pit resistance at high P_a and an inherent limit to tracheid length. To test this, we set L to 5 mm, which was the observed length for tracheids of the maximum 51 μm diameter (Fig. 11A). As expected, these length-limited tracheids lost more conductivity as P_a increased, because they become progressively shorter than their saturating length (Fig. 12, compare wide–short line with wide line). However, this cannot be the only reason for the observed trend for narrower tracheids with increasing P_a (Fig. 6B), because even if wide tracheids were shorter than their saturating length, they were still substantially more efficient than narrow ones at their saturating length (Fig. 12).

Maximum possible tracheid K_{sc}—To find the pit dimensions that maximized tracheid K_{sc}, we computed the K_{sc} for a wide range of pit diameters from a minimum of 3 μm to a maximum equal to D_c. For each D_m setting, we varied the aperture diameter from a minimum of D_a = 1 μm to a maximum of (D_m − 1 μm). The torus diameter (D_t) was calculated from the average torus overlap for the data set of 0.28 (Fig. 9). All other parameters were kept constant at the value for the average tracheid. The optimal combination of pit dimensions maximized the tracheid K_{sc}. We repeated this analysis independently at each tracheid length setting (Fig. 13A; open symbols). The maximum K_{sc} was then compared with the ''actual'' tracheid K_{sc} for average tracheids (Fig. 13A; solid symbols).

The maximum tracheid K_{sc} exceeded the actual K_{sc} across all length settings (Fig. 13A, compare open vs. closed symbols). However, the actual K_{sc} rose to within 95% of the maximum near the saturating tracheid length (Fig. 13B, arrow). Thus, actual pit dimensions most closely matched the optimum at what one would assume to be the optimal length setting—the saturated length. The optimum pit membrane diameter for the saturated length of 2 mm was 18.5 μm with D_a = 3.5 μm.

Actual pits had a similar aperture diameter (D_a = 3.6 μm), but smaller membrane size (D_m = 12.9 μm).

The same conclusion was reached in our analysis of vessels, except that tracheids came 7% closer to the optimum at their saturated length. In both conduit types, the optimal pit size was relatively large, because large pits mean higher ligament efficiencies and thinner walls, leading to less wall area for a given implosion resistance and lumen conductivity. The larger size of tracheid vs. vessel pits (Fig. 5B) resulted in tracheids coming closer to the maximum possible conduit K_{sc}.

DISCUSSION

The results provided theoretical answers to our three questions of the introduction, the first being whether the torus-margo membrane of gymnosperm tracheids is more or less conductive than the homogenous pit membranes of vessels. The torus-margo membrane has 3.3 to 43 times higher conductivity per membrane area than the homogenous pit membrane (Fig. 8A). The reason was primarily in the much greater membrane conductivity per area, which also showed relatively little decrease with increasing air-seed pressure as compared to the vessel pit membrane (Fig. 8B). This result supports the intuition of Lancashire and Ennos (2002), who, after measuring the hydraulic conductivity of physical models of the conifer pit membrane, speculated that it must be more conductive than the vessel type.

The efficiency of the torus-margo membrane is the direct consequence of the larger pores possible in the margo compared to the homogenous vessel pit membrane. Capillary forces at these pores are only required to aspirate the membrane so that the torus can seal the aperture (Petty, 1972). They do not have to provide the ultimate seal against air entry as they must in the vessel membrane (Fig. 1B). Being larger, the pores are much more conductive, there being a roughly third-power relationship between pore diameter and conductivity (Vogel, 1994). Even though there are fewer membrane pores because of a torus, this was more than made up by the greater pore size. In fact, the torus must become much wider than it was to cause a significant decrease in membrane conductivity (Fig. 9).

Interestingly, narrowing the torus also caused the membrane conductivity to decrease—even though a smaller torus created relatively more margo area (Fig. 9). The reason was that a greater number of margo strands were required to hold the narrower torus in sealing position. More margo strands mean smaller pores and lower membrane conductivity. The observed torus size relative to the rest of the pit appeared to optimize the membrane conductivity by maximizing the size and number of margo pores.

The torus width also has implications for the mode of air-seeding. A relatively narrow torus is more likely to stretch the margo to the aperture without breaking it, causing stretch-seeding. Conversely, a wide torus is more likely to break the margo and cause rupture-seeding (Figs. 7, 9). Based on our mechanical model, we predicted that the ratio of the membrane spoke strength to elastic modulus (F/E) must exceed 0.4 for stretch-seeding to occur for observed torus dimensions. The corresponding ratio for vessel pits from the companion paper (Sperry and Hacke, 2004) was only approximately 0.1, meaning that the gymnosperm pit must have about four times greater microfibril strength than the vessel pit to avoid rupture-seeding for the same elastic modulus. The higher value for gymnosperm pits is because we assumed all membrane strain was located in the margo and the gymnosperm pits were so much larger in size than the vessel pit.

Unfortunately, we know little about the actual mechanical properties of the pit membrane. We also know little about whether the actual mode of air-seeding is by elastic stretching or by rupture-seeding. It seems likely that the air-seeding may occur beyond the elastic limit, because Petty (1972) concluded that because cellulose microfibril creep can occur at a strain of 0.01, the typical aspiration strain of approximately 0.03 should cause at least temporarily irreversible stretching. This may be why pits can become stuck in an aspirated condition, particularly when the xylem is subjected to prolonged or severe water stress (Petty, 1972). However, pits briefly aspirated by hydraulic pressure can rebound (Sperry and Tyree, 1990). It seems unlikely that the margo strands are completely broken in half during air-seeding, because conifers in nature appear to go through embolism and refilling cycles (Sperry et al., 1994; Mayr et al., 2002). We do not know whether the phenomenon of ''cavitation fatigue'' (Hacke et al., 2001b) extends to the torus-margo type of pit membrane. Although for lack of other information we assumed the same F and E values for both torus-margo and homogenous membranes, the analysis suggests that at least the F/E ratios are probably much lower for the vessel type of membrane. If so, this could be one reason for the generally smaller size of vessel pits (Fig. 5B).

The second question from the introduction concerned how the tracheids and vessels compared with respect to resistance to implosion by negative pressure and hydraulic efficiency. Tracheids, especially stem tracheids, had higher safety factors (average P_i/P_a = 4.8 for stems) from implosion than vessels (average P_i/P_a = 1.8; Fig. 4A). Vessels are presumably buffered to some extent against extra mechanical stress by fibers. The extra reinforcement of tracheids was expected, given that tracheids must transport water *and* strengthen the axis. The greater reinforcement of stem vs. root tracheids was also expected, given the greater structural demands of gravity and wind on the freestanding stem in comparison to roots that are supported by the surrounding soil. Without such reinforcement, negative xylem pressures could significantly weaken the stem against breakage by wind. It is an interesting question if drought stress could lead to greater vulnerability to stem breakage by increasing the stress in tracheid walls, even given their added wall thickness.

As for vessels, the scaling between implosion and air-seed pressures in tracheids was achieved by an increase in thickness-to-span ratio of the tracheid with air-seed pressure (Fig. 4B, solid symbols). Tracheid pits weakened the wall by an average of 30%. This is similar to the 20–40% figure for vessel pits, the only difference being that the larger pit chambers of tracheid pits accounted for 5% of the weakening vs. having no effect in the smaller vessel pits. Our model did not account for the typical bulge of the pit border toward the tracheid lumen of gymnosperm pits. Such a bulge could make the pits stronger than our analysis predicted by moving the pit border farther from the neutral axis of bending. The relatively thicker walls of tracheids mean that they are potentially less efficient conductors of water on a wall area basis than vessels. However, if the considerable wall area devoted to fibers is considered, water transport in gymnosperms is actually cheaper in terms of wood density and the metabolic cost of wood production (Hacke et al., 2001a).

The tracheids of pine needles appear to behave quite dif-

ferently from what our analysis suggests for those in stems and roots. Needle tracheids appear to undergo a controlled and reversible wall collapse without causing cavitation (Cochard et al., 2004). The collapse is not initiated by the bending stresses we analyzed, but by hoop stresses in water-filled tracheids that seem to trigger folding at thin areas in the wall. This interesting phenomenon may be adaptive in shutting down water transport and initiating stomatal closure without cavitation. The tracheids in pine stems behaved as expected from our results, cavitating before showing any signs of collapse (Cochard et al., 2004). Collapsing conduits may be a special adaptation limited to tissues not involved in mechanical support and to a conduit structure that can accommodate wall folding without disrupting vascular continuity.

An important prediction of the model is that, aside from differences in thickness-to-span ratio, tracheids and vessels should be of equal hydraulic conductivity—as long as they are of equal diameter and as long as they can achieve their saturated length (Fig. 11B). The conductivity of conduits at the saturated length is no longer influenced by pit conductivity—only by the dimensions of wall and lumen (Eq. 15). Although much is made of the greater hydraulic conductivity of vessels, there is, in fact, a considerable overlap in hydraulic conductivity per total xylem area between coniferous and angiosperm woods (Tyree and Zimmermann, 2002). This observation has been recently emphasized in a comparison of vesselless vs. vessel-bearing angiosperm woods (Becker et al., 1999; Feild et al., 2002). Vessel-based wood is not always more conductive than tracheid-based wood.

According to our model, vessels will be more conductive than tracheids only if they achieve wider diameters and maintain a correspondingly longer saturating length. There is no obvious developmental limitation on vessel length, and vessel diameters can exceed 0.5 mm, in part because the surrounding fibers make room for the lateral expansion of the developing vessel members. Tracheid diameter, on the other hand, has at least two limitations. First, tangential expansion of the tracheid is seemingly limited by the width of the fusiform initials. The tracheids exist side-by-side tangentially, and if all expand uniformly, they will distort the cambium. Vessels can expand to large diameters at the expense of the thinning of fibers and parenchyma that surround them. Second, because tracheids develop from a single cell, their length is limited. For gymnosperm trees, the maximum average length is approximately 5–6 mm (Panshin and de Zeeuw, 1970). As has been pointed out before (Calkin et al., 1986; Gibson et al., 1986; Schulte et al., 1987; Schulte and Gibson, 1988), and further quantified here, if conduits cannot increase in length as they increase in diameter, their conductivity will eventually stop increasing because it becomes limited by the conductivity of the pitted walls. For a maximum tracheid length of 5 mm, the model predicts no further increase in tracheid conductivity for an increase in diameter beyond approximately 70–80 μm (Fig. 11B, dashed line). This is also essentially the limit of tracheid diameters in coniferous woods (Panshin and de Zeeuw, 1970).

Several points of evidence indicate that tracheids of the average diameter for our data set (19 μm) are near the saturating length required to maximize tracheid conductivity. A priori, the saturated length is optimal because a longer length provides no significant gain in conductivity of functional tracheids and causes greater loss of conductivity from embolism (Comstock and Sperry, 2000) and a shorter length sacrifices conductivity. The conductivity of the average tracheid came closest to the maximum possible conductivity at lengths near the saturating length, suggesting the pit structure was ''tuned'' for tracheids of the saturating length (Fig. 13). Most importantly, predicted saturating lengths agreed well with measured lengths for tracheids near the average diameter (Fig. 11A, compare measured vs. modeled lines at D_c = 19 μm). Notably, the greater conductivity of the torus-margo tracheid pit relative to the vessel pit resulted in the saturating lengths of tracheids being 1.7–3.4 times shorter than for vessels over a diameter range of 25–50 μm (Fig. 11A).

Figure 11A indicates that above a diameter of about 30 μm, tracheids fall progressively short of their optimal saturating length and become increasingly pit limited. According to Lancashire and Ennos (2002), a conifer tracheid 40 μm in diameter will have 29% of its resistance in pits—consistent with it being about 25% short of its optimal length in our analysis (Fig. 11A, compare measured vs. modeled lengths at D_c = 40 μm). This trend is symptomatic of a limitation on tracheid length and as noted above, it is a trend of diminishing returns. Ultimately the pit resistance will prevent further increases in tracheid diameter from significantly altering conductivity (e.g., Fig. 11B, dashed line).

The predicted decline in tracheid conductivity with air-seed pressure (Fig. 12) was enhanced by the observed decline in tracheid diameter with air-seed pressure (Fig. 6B). Vessel diameter, by contrast, did not decline with air-seed pressure (Fig. 6B). It is reasonable to propose that the decline in tracheid diameter is caused by a greater limitation of pit conductivity with increasing air-seed pressure. Less conductive pits require longer tracheids to reach the saturating tracheid conductivity. Length limitations thus could rule out the combination of wide tracheids with high air-seed pressures. According to the model results, however, this alone cannot account for the observed trend because even if length was limited in the model, wide tracheids at high air-seed pressures still had a higher conductivity than the narrow measured tracheids (Fig. 12). Perhaps what limits tracheid diameter at high air-seed pressures is the sheer amount of wall material that must be put into place during tracheid development. A large diameter tracheid with a high air-seed pressure will require much more wall material per cell (to maintain implosion strength) than if it had a low air-seed pressure. Thus, limited cell wall synthesis per cell could translate into limits on tracheid size with increasing air-seed pressure (T. Speck, University of Freiburg, personal communication).

The tracheid vs. vessel comparison raises an interesting question. If the torus-margo pit of gymnosperms is so much more conductive than the homogenous pit of a vessel, then why don't vessels have torus-margo pitting? It is true that a few angiosperms do have what is presumably the functional equivalent of a torus-margo pit membrane (Wheeler, 1983), but most do not. The answer may be that because vessel length is unlimited, the relatively low conductivity of vessel pits can be rendered inconsequential by making longer vessels that achieve their lumen-saturated conductivity. Putting a more efficient pit in such lumen-limited vessels should cause little or no increase in vessel conductivity. Conversely, because tracheid length is limited, switching out a torus-margo pit for a vessel pit could cause a substantial drop in tracheid conductivity.

To test this explanation, we calculated the change in vessel conductivity caused by switching from vessel-type pits to torus-margo pits. Only the pit membrane and pit dimensions

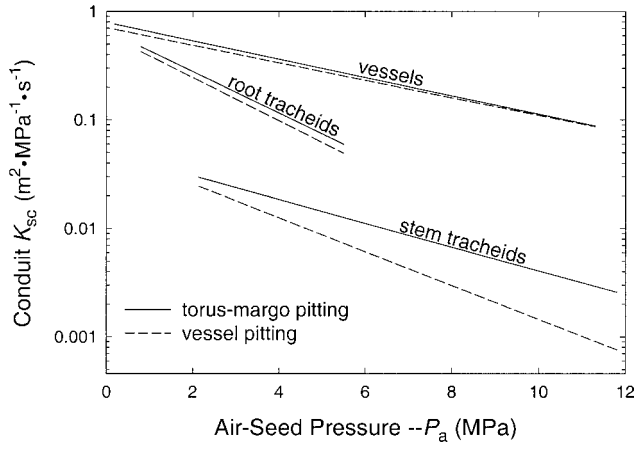

Fig. 14. Conduit K_{sc} vs. air-seed pressure (P_a) for vessels and tracheids with torus-margo pitting (solid lines) vs. with homogenous pit membranes of vessel pitting (dashed lines). Only the regression lines through the data sets are shown for clarity. The regressions for conduits with native pit types (vessels with vessel pits; tracheids with torus-margo pits) are for the same data shown in Fig. 12. To switch from the native pitting, only the pit membrane and pit dimensions were altered to match the alternate pit type. Conduit length was constant at the saturating length for the native pit type, and conduit P_i/P_a scaling was constant at the native condition.

were altered to match conifer pitting. Conifer pit dimensions followed the observed scaling with air-seed pressure (Fig. 6A) and torus proportions (Fig. 5B). Otherwise, the vessel length was kept at the saturating length for vessel pitting, and the vessel P_i/P_a scaling (Fig. 4A, dashed vessel line) was retained. Vessel conductivity increased on average by a modest 8% as a result of the switch to conifer pitting (Fig. 14, compare dashed vs. solid line for vessels). This increase was primarily because of the larger pit dimensions of conifers and hence thinner walls for the same implosion pressure rather than any direct effect of increased pit conductivity.

Conversely, we also estimated the change in tracheid conductivity resulting from switching to vessel-type pits. Vessel pits were of the average diameter (D_m = 4.9 μm), with aperture diameters following the scaling with air-seed pressure previously reported (Fig. 7A in Sperry and Hacke, 2004). Otherwise, tracheid length was held constant at the saturating length for tracheid pitting, and the tracheid P_i/P_a scaling (Fig. 4A) was followed. Changing to vessel pitting caused tracheid conductivity to decrease by 15% for root tracheids and 41% for stem tracheids. The decrease was due to tracheid lengths becoming shorter than the saturating length required of low conductivity vessel pits and to the thicker walls required to achieve the implosion pressure for the smaller pits of vessels. The greater effect in stem tracheids was primarily because of their shorter lengths vs. root tracheids. In addition, the disparity between the conductivity of vessel vs. torus-margo pitting increased with increasing air-seed pressure, and stem tracheids had higher air-seed pressures than root tracheids (Fig. 14).

The implication is that the unique torus-margo pit structure is essential for maintaining hydraulic conductivity in length-limited gymnosperm tracheids. It seems doubtful that giant sequoias and towering redwoods could exist without torus-margo pitting, because it would cut their stem conductivity nearly in half! The lack of a length limitation in vessel structure relaxes the requirement for maximally efficient pits, hence the lack of a torus-margo structure in most vessel pitting.

It follows that tracheids that lack the high-conductivity torus-margo membrane, such as those in pteridophytes, cycads, and vesselless angiosperms, are potentially more pit limited for their size than tracheids with the modified membrane. Based on conductivity measurements made before and after pit membrane digestion with cellulases, Schulte and Gibson (1988) estimated a pit resistance between 11.6 and 60% for species of *Ruscus*, *Drimys*, *Trochodendron*, and *Dioon*; all possessing tracheids with homogenous membranes. The pit limitation was greatest in species with the largest tracheid diameters. Many of these species exhibited scalariform pitting, a geometry not compatible with the function of the torus-margo membrane, but one that should be more efficient in maximizing pit membrane area per wall area. This pitting geometry, and possibly longer tracheid lengths, could compensate to some extent for the lower pit membrane conductivity. Of course, so could the evolution of vessels, which (not coincidentally, we suggest) has occurred in most if not all cases from tracheid-bearing ancestors that lack the torus-margo membrane organization.

The third question of the introduction was how closely the actual gymnosperm pit and tracheid structure comes to achieving the maximum possible conducting efficiency. We found that tracheids at their saturated lengths came within 5% of the maximum possible tracheid K_{sc} for that length obtained by iterating through the range of possible pit dimensions (Fig. 13). This is somewhat superior to vessels, which came within 12% of their maximum possible conductivity at the saturating length. Maximum possible conductivities were associated with large diameter pits (which allowed for thinner walls for the same implosion pressure). The larger pit dimensions of tracheids vs. vessels were thus responsible for their closer approach to the theoretical maximum conductivity.

In summary, our results imply that vessels should achieve a higher conductivity than tracheids only when pit conductivity becomes limiting for tracheids. A pit limitation can arise by at least three ways. (1) Low conductivity pitting, such as is seen in the homogenous pit membranes of vessels but also of tracheids in the vesselless angiosperms, ferns, and other groups. A need for high air-seed pressures for the colonization of arid habitats would also create low pit conductivity. (2) A wood structure permitting the lateral expansion of tracheary elements so that large lumen diameters can be achieved. Multiple cell types such as fibers and axial parenchyma are probably necessary to permit the expansion of individual tracheary elements to a diameter significantly greater than the width of a fusiform initial cell. (3) Any limitation to tracheid length such as resistance to intrusive growth or limitations on total cell volume or wall synthesis capability. When these factors combine to prevent tracheids from achieving their saturating lengths, vessels should be more advantageous.

The strength of our conclusions naturally rests on the validity of the model, and many components—perhaps most importantly the pit and conduit conductivity estimates—remain to be directly tested. Nevertheless, the conceptual and comparative results across air-seed pressure and across gymnosperm vs. angiosperm pit types should be fairly robust. We hope that the theoretical and comparative approach we have taken stimulates further research by providing quantitative hypotheses of pit and conduit function.

LITERATURE CITED

ASHBY, M. F., L. J. GIBSON, U. WEGST, AND R. OLIVE. 1995. The mechanical properties of natural materials. I. Material property charts. *Proceedings of the Royal Society of London, Series A* 450: 123–140.

BAUCH, J. W., W. LIESE, AND R. SCHULTZE. 1972. The morphological variability of the bordered pit membranes in gymnosperms. *Wood Science and Technology* 6: 165–184.

BECKER, P., M. T. TYREE, AND M. TSUDA. 1999. Hydraulic conductances of angiosperms versus conifers: similar transport sufficiency at the whole-plant level. *Tree Physiology* 19: 445–452.

CALKIN, H. W., A. C. GIBSON, AND P. S. NOBEL. 1986. Biophysical model of xylem conductance in tracheids of the fern *Pteris vittata*. *Journal of Experimental Botany* 37: 1054–1064.

COCHARD, H., F. FROUX, S. MAYR, AND C. COUTAND. 2004. Xylem wall collapse in water-stressed pine needles. *Plant Physiology* 134: 1–8.

COMSTOCK, J. P., AND J. S. SPERRY. 2000. Tansley review no. 119. Some theoretical considerations of optimal conduit length for water transport in plants. *New Phytologist* 148: 195–218.

DAGAN, Z., S. WEIBAUM, AND R. PFEFFER. 1982. An infinite-series solution for the creeping motion through an orifice of finite length. *Journal of Fluid Mechanics* 115: 505–523.

DOMEC, J.-C., AND B. L. GARTNER. 2002. How do water transport and water storage differ in coniferous earlywood and latewood? *Journal of Experimental Botany* 53: 2369–2379.

FEILD, T. S., T. BRODRIBB, AND N. M. HOLBROOK. 2002. Hardly a relict: freezing and the evolution of vesselless wood in Winteraceae. *Evolution* 56: 464–478.

GIBSON, A. C., P. J. SCHULTE, AND P. S. NOBEL. 1986. Water-flow and hydraulic conductance in stems of *Psilotum nudum*. *American Journal of Botany* 73: 650–650.

HACKE, U. G., J. S. SPERRY, B. E. EWERS, D. S. ELLSWORTH, K. V. R. SCHÄFER, AND R. OREN. 2000. Influence of soil porosity on water use in *Pinus taeda*. *Oecologia* 124: 495–505.

HACKE, U. G., J. S. SPERRY, W. P. POCKMAN, S. D. DAVIS, AND K. A. MCCULLOH. 2001a. Trends in wood density and structure are linked to prevention of xylem implosion by negative pressure. *Oecologia* 126: 457–461.

HACKE, U. G., V. STILLER, J. S. SPERRY, J. PITTERMANN, AND K. A. MCCULLOH. 2001b. Cavitation fatigue: embolism and refilling cycles can weaken cavitation resistance of xylem. *Plant Physiology* 125: 779–786.

HEPWORTH, D. G., AND J. F. V. VINCENT. 1998a. Modelling the mechanical properties of xylem tissue from tobacco plants (*Nicotiana tabacum* ''Samsun'') by considering the importance of molecular and micromechanisms. *Annals of Botany* 81: 761–770.

HEPWORTH, D. G., AND J. F. V. VINCENT. 1998b. The mechanical properties of xylem tissue from tobacco plants (*Nicotiana tabacum* ''Samsun''). *Annals of Botany* 81: 751–759.

HUBBARD, R. M., V. STILLER, M. G. RYAN, AND J. S. SPERRY. 2001. Stomatal conductance and photosynthesis vary linearly with plant hydraulic conductance in ponderosa pine. *Plant, Cell and Environment* 24: 113–121.

JERONIMIDIS, G. 1980. Wood, one of nature's challenging composites. *In* J. D. Curry [ed.], The mechanical properties of biological materials, 169–182.Cambridge University Press, Cambridge, UK.

KAVANAGH, K. L., B. J. BOND, S. N. AITKEN, B. L. GARTNER, AND S. KNOWE. 1999. Shoot and root vulnerability to xylem cavitation in four populations of Douglas-fir seedlings. *Tree Physiology* 19: 31–37.

LANCASHIRE, J. R., AND A. R. ENNOS. 2002. Modelling the hydrodynamic resistance of bordered pits. *Journal of Experimental Botany* 53: 1485–1493.

LINTON, M. J., J. S. SPERRY, AND D. G. WILLIAMS. 1998. Limits to water transport in *Juniperus osteosperma* and *Pinus edulis*: implications for drought tolerance and regulation of transpiration. *Functional Ecology* 12: 906–911.

MARK, R. E. 1967. Cell wall mechanics of tracheids. Yale University Press, New Haven, Connecticut, USA.

MAYR, S., M. WOLFSCHWENGER, AND H. BAUER. 2002. Winter-drought induced embolism in Norway spruce (*Picea abies*) at the Alpine timberline. *Physiologia Plantarum* 115: 74–80.

PANSHIN, A. J., AND C. DE ZEEUW. 1970. Textbook of wood technology. McGraw Hill, New York, New York, USA.

PETTY, J. A. 1972. The aspiration of bordered pits in conifer wood. *Proceedings of the Royal Society of London, Series B* 181: 395–406.

POCKMAN, W. T., AND J. S. SPERRY. 2000. Vulnerability to xylem cavitation and the distribution of Sonoran Desert vegetation. *American Journal of Botany* 87: 1287–1299.

SCHULTE, P. J., AND A. C. GIBSON. 1988. Hydraulic conductance and tracheid anatomy in six species of extant seed plants. *Canadian Journal of Botany* 66: 1073–1079.

SCHULTE, P. J., A. C. GIBSON, AND P. S. NOBEL. 1987. Xylem anatomy and hydraulic conductance of *Psilotum nudum*. *American Journal of Botany* 74: 1438–1445.

SPERRY, J. S., AND U. G. HACKE. 2004. Analysis of circular bordered pit function. I. Angiosperm vessels with homogenous pit membranes. *American Journal of Botany* 91: 369–385.

SPERRY, J. S., AND T. IKEDA. 1997. Xylem cavitation in roots and stems of Douglas-fir and white fir. *Tree Physiology* 17: 275–280.

SPERRY, J. S., K. L. NICHOLS, J. E. M. SULLIVAN, AND S. E. EASTLACK. 1994. Xylem embolism in ring-porous, diffuse-porous, and coniferous trees of northern Utah and interior Alaska. *Ecology* 75: 1736–1752.

SPERRY, J. S., AND M. T. TYREE. 1990. Water-stress-induced xylem embolism in three species of conifers. *Plant Cell and Environment* 13: 427–436.

TIO, K. K., AND S. S. SADHAL. 1994. Boundary conditions for stokes flows near a porous membrane. *Applied Scientific Research* 52: 1–20.

TYREE, M. T., AND M. H. ZIMMERMANN. 2002. Xylem structure and the ascent of sap. Springer, Berlin, Germany.

VOGEL, S. 1994. Life in moving fluids: the physical biology of flow. Princeton University Press, Princeton, New Jersey, USA.

WHEELER, E. A. 1983. Intervascular pit membranes in *Ulmus* and *Celtis* native to the USA. *International Association of Wood Anatomists Bulletin* 4: 79–88.

YOUNG, W. C. 1989. Roark's formulas for stress and strain. McGraw Hill, New York, New York, USA.